Journal of Renewable Materials

Tech Science Press

DOI: 10.32604/jrm.2022.020215

ARTICLE

# Magnetic Wakame-Based Biochar/Ni Composites with Enhanced Adsorption Performance for Diesel

**Hua Jing[1], Shiyao Lu[1], Lili Ji[1,*], Shijie Li[1], Baikang Zhu[2], Jian Guo[3], Jiaxing Sun[1], Lu Cai[4] and Yaning Wang[1]**

[1]National Marine Facilities Aquaculture Engineering Technology Research Center, Zhejiang Ocean University, Zhoushan, 316022, China

[2]College of Petrochemical Engineering and Environment, Zhejiang Ocean University, Zhejiang Ocean University, Zhoushan, 316022, China

[3]College of Food and Medical, Zhejiang Ocean University, Zhoushan, 316022, China

[4]Institute of Ocean Higher Education, Zhejiang Ocean University, Zhoushan, 316022, China

[*]Corresponding Author: Lili Ji. Email: jll-gb@163.com

Received: 11 November 2021 Accepted: 24 January 2022

## ABSTRACT

In this study, the magnetic wakame biochar/Ni composites were prepared with three activating reagents of $H_3PO_4$, $ZnCl_2$ and KOH by one-step pyrolysis activation, characterized by BET, SEM, TEM, FI-IR, XRD, Raman, and elemental analyzer, and their adsorption performance for diesel were also analyzed. The results showed that wakame biochar/Ni composites had larger specific surface area, abundant porous structure, and various reactive groups, rendering its enhancement of adsorption efficiency. The adsorption experiments indicated that the maximum adsorption capacities for diesel using WBPA 0.5, WBHZ 0.5 and WBPH 0.5 were 4.11, 8.83, and 13.47 g/g, respectively. The Langmuir model was more suitable for the adsorption isotherms process, and the Pseudo-second-order model could better describe the adsorption kinetic experimental. And the magnetic wakame biochar/Ni composites presented good stability and recyclability. This study provides a novel pattern for the high-value utilization of wakame, having huge potential in the treatment of oily wastewater.

## KEYWORDS

Wakeme; magnetic biochar/Ni composites; activating reagents; diesel adsorption

## 1 Introduction

With the rapid development of economy and industrialization, the production and consumption of petroleum products are increasing worldwide, and as a side effect of transportation, exploration and related processes, oil spill is unfortunately increasing accordingly [1,2]. Water resources and petroleum resources are indispensable in human life and industrial development, but the harm and pollution caused by oily pollutants to water resources are becoming seriously [3–5]. Oily pollutants mainly include alkane and naphthene, crude oil components of aromatic and asphaltene [6]. It is well known that aromatic compounds have strong toxicity and poor biodegradability (such as polyaromatic hydrocarbons), and complex hydrocarbons such as polycyclic isoprenoids are persistent in the environment (such as terpenes)

[7,8]. These oily pollutants cause serious problems to the animals and plants in the water and residents nearby, seriously threatening their health and quality of life [9], and may cause chronic rhinosinusitis and airway disorders [10], lung diseases, cancer and skin diseases [11]. Therefore, the removal and recovery of oily pollutants in water has attracted widespread attention in the research field.

Up to date, there is a variety of methods available for the treatment of oily wastewater, mainly including physical, chemical and biological method [12]. Physical method commonly employs oil booms, skimmers or sorbents to remove oil from water [13], oil dispersant as a chemical method is often used in the treatment of oily waste [14] and biological method uses petroleum-degrading microorganism to eliminate oil pollutants [15]. Among these, the treatment of oily wastewater by sorbent has been considered as an economically feasible, effective, facile-operating and no secondary pollution method [16,17], and there has been various sorbents employed to remove oil pollutant from water, such as activated carbon [18], kaolin [19], silica [20], fly ash [21], etc. However, most sorbents for the treatment of oily wastewater have been confronted with the challenges of low efficiency and poor reutilization.

In recent years, with the increasingly prominent energy crisis, the preparation of biochar materials from cheap, readily available, and renewable biomass in nature has attracted increasing attention [22,23]. The biomass materials for the preparation of biochar have been ranged from the first-generation agricultural wastes (such as straw, corn cob, bagasse) [24] to the second-generation forestry wastes (such as lignocellulose) [25]. At present, it has been transferred from land to lake and ocean, especially microalgae and macroalgae with high biomass and short growth cycle [26], have become the third generation of biomass carbon sources. And algal biochar, as a new kind of biomass carbon-based material, has been used in various fields, such as in the soil remediation [27], wastewater treatment [28] and lithium battery and sensor [29,30]. Generally, biochar could be prepared with various methods, including pyrolysis, hydrothermal carbonization, flash carbonization, and gasification [31], and activation is a crucial step in the preparation of biochar, which can form porous structure, enlarge specific surface area, increase surface active groups and change surface hydrophilicity or hydrophobicity, rendering the improvement of the physicochemical properties [32]. And physical activation and chemical activation are the common methods applied in the activation process, among which, chemical activation is a series of cross-linking or polycondensation reactions between chemical reagents (acid, alkali, and oxidation) with carbon materials to create abundant porous structures, possessing short activation time, low activation temperature and high productive rate, and so on [33]. However, there are still some practical problems to overcome in the application of biochar, it is difficult to separate and recovery effectively due to its small particles, which limits its large-scale application. Recently, magnetic separation technique has been introduced in the preparation of biochar, transition metals (Fe, Ni, etc.) or their oxides have been employed to prepare magnetic biochar [34,35], which can simply and rapidly realize the separation and recovery of biochar in a magnetic field.

In this study, a series of novel magnetic biochar/Ni composites derived from wakame were synthesized with three different activators (KOH, $ZnCl_2$ and $H_3PO_4$) by a facile and effective impregnation-pyrolysis method. The as-prepared samples were characterized by BET, SEM, TEM, FI-IR, XRD, Raman, and elemental compositions were also analyzed. Moreover, the adsorption performances for diesel wastewater using as-prepared samples were investigated by batch adsorption experiments, and the adsorption isotherms, kinetics and thermodynamics of as-prepared samples for diesel were also studied to further analyze its adsorption mechanism. Then, the magnetic recovery cycle experiments of as-prepared samples were carried out in an extra magnetic field. This study would provide a novel promising bio-absorbent prepared by macroalgae in the treatment of oily wastewater.

## 2 Materials and Methods

### *2.1 Materials*

The wakame used in this study was purchased from Yantai City, Shandong Province, China. The wakame was washed and soaked in tap water several times to remove the salt in the wakame, and dried

at 85°C. Diesel (Sinopec), Potassium hydroxide (KOH), zinc chloride ($ZnCl_2$), phosphorus pentoxide ($P_2O_5$) and nickel chloride hexahydrate ($NiCl_2$•$6H_2O$) were all purchased from Shanghai Sinopharm Chemical Reagent Co., Ltd., China All reagents used in the experiment are of analytical grade and no further purification is required.

### *2.2 Preparation of Magnetic Biochar/Ni Composites*

According to our previous work [36], 5.0 g of wakame powder were added to 50 mL 0.5 mol/L $NiCl_2$ solution, stirred by ultrasonic for 4 h, stood for overnight and filtered, and the underlayer precipitation was taken and dried. And then, mix 50 mL of activators (KOH, $ZnCl_2$ and $H_3PO_4$) with the pretreated wakame powder above, where the mass ratio of activator to wakame: activator/wakame (w/w) = 0.5:1 or 1:1, respectively, which were stirred at 80°C for 2 h, filtered and dried in an oven at 105°C for 12 h. The dried sample was transferred to a tube furnace, heated to 800°C at a rate of 10 °C/min under nitrogen atmosphere condition (with a flow rate of 100 mL/min), and kept at 800°C for 2 h. After cooling, the obtained magnetic wakame biochar was washed with deionized water to pH = 7, and dried in an oven at 85°C for 12 h. The as-prepared samples with KOH activation were denoted as WBPH 0.5 and WBPH 1, those with $ZnCl_2$ activation are denoted as WBHZ 0.5 and WBHZ 1 and those with $H_3PO_4$ activation were denoted as WBPA 0.5 and WBPA 1. For comparison, the magnetic biochar that was carbonized at 800°C without any activator was labeled as MWB.

### *2.3 Characterization of Magnetic Biochar/Ni Composites*

$N_2$ adsorption/desorption isotherm was performed on a static volumetric adsorption analyzer (Micromeritics ASAP 2010, Shanghai, China) and calculated with the method of Brunauer-Emmett-Teller (BET). The microstructure and surface morphology of as-prepared sample was observed by scanning electron microscope (SEM, S4800, Hitachi, Japan) and transmission electron microscope (TEM, Joel-2100, JEOL, Japan). The element analyzer was used to determine the contents of organic elements (C, H, N, S and N) of as-prepared sample, and the content of metallic nickel was obtained by inductively coupled plasma emission spectrometer (ICP-OES; ICAP6000, Thermo Fisher Scientific, USA). The X-ray diffraction (XRD) patterns were recorded on an X-ray Diffractometer (Ultima IV, Rigaku Corporation, Japan) in the range of 2θ from 20 to 80°. The Raman spectra were recorded by Raman spectroscopy using a 532 nm excitation wavelength (InVia-Reflex, Renishaw, UK). At the same time, the surface functional groups of as-prepared sample were analyzed by Fourier transform infrared spectroscopy (FTIR, Nicoletteis 50, Thermo Fourier, USA). And the magnetic properties were studied using a vibrating Specimen magnetometer (VSM, 7407, Lakeshore, USA).

### *2.4 Batch Adsorption Experiments*

0.1 g of magnetic biochar/Ni composites (MWB, WBPH 0.5, WBPH 1, WBHZ 0.5, WBHZ 1, WBPA 0.5 and WBPA 1) were added into 50 mL (2%, 4%, 8%, 16% and 20%) diesel solution for batch adsorption experiments, respectively, which was put into a water bath thermostatic oscillator and oscillate at 25°C for 3 h. And then under external magnetic field, the adsorbent was separated from the mixed solution at 5, 10, 20, 30, 60, 90, 120 and 180 min, respectively, and the adsorbed diesel by as-prepared sample was recovered and weighed. Moreover, the effects of diesel initial concentration and absorbent dose on the adsorption capacities of diesel were also investigated.

To evaluate the stability of the prepared adsorbent, the repeat cycle experiments were also performed. The magnetic biochar/Ni composite with adsorbed diesel was added into ethanol for desorption. The as-prepared adsorbent was recovered by magnetic separation, and dried in an oven at 85°C for 12 h. The cycles of adsorption-magnetic separation-desorption were carried out for 5 times.

The adsorption efficiency of magnetic biochar/Ni composite to diesel was calculated according to Eq. (1):

$$q_t = \frac{W_t - W_0}{W_0} \tag{1}$$

where $q_t$ (%) is the adsorption rate of diesel by adsorbent, $w_t$ (g) is the weight of the adsorbent after adsorbing diesel, and $w_0$ (g) is the initial weight of the adsorbent.

### *2.5 Statistical Analysis*

Statistical analysis was performed using Origin 8.5 (Origin Corp., USA); Jade 6.0 was used to process the XRD data.

## 3 Results and Discussion

### *3.1 Characterization of Magnetic Biochar/Ni Composites*

#### *3.1.1 Porous Structure*

The $N_2$ adsorption-desorption isotherm was employed to determine pore characteristics of the as-prepared samples. As shown in Fig. 1, it can be seen that MWB, WBPA, WBHZ and WBPH conform to the IV isotherm model. After activation, $N_2$ adsorption capacities of magnetic biochar/Ni composites significantly enhance, and WBPA 0.5, WBHZ 0.5 and WBPH 0.5 possess higher $N_2$ adsorption capacities compared with WBPA 1, WBHZ 1 and WBPH 1. There are wide hysteresis loops between their adsorption and desorption branches ($P/P_0 > 0.4$), indicating the existence of mesoporous structure [37]. However, the hysteresis loop of WBN failed to close, which may be caused by an irreversible reaction during the adsorption-desorption process [38]. As shown in Table 1, the specific surface area and pore volume of magnetic biochar/Ni composites obviously increase after activation, among which, those of WBPH are maximum, followed by those of WBHZ and WBPA, indicating KOH is the optimum activator for the preparation of magnetic biochar/Ni composite. And the specific surface area and pore volume of WBPA 0.5, WBHZ 0.5 and WBPH 0.5 are higher than those of WBPA 1, WBHZ 1 and WBPH 1, and those of WBPH 0.5 are highest, up to 824.174 $m^2/g$ and 0.445 $cm^3/g$, respectively. As the ratio of activator increases, the specific surface area and pore volume of magnetic biochar/Ni nanocomposite decrease, probably because more activator could consume more carbon of wakame, and further destroy pore structure of magnetic biochar/Ni composite.

Based on $N_2$ adsorption-desorption data, the non-local density functional theory (NLDFT) model is used to calculate pore size distribution (PSD) of as-prepared sample, it can be demonstrated that the PSD of magnetic biochar/Ni composites are in the range of 3.8-4 nm, belonging to mesoporous materials. It has been demonstrated that $H_3PO_4$, $ZnCl_2$ and KOH as activators applied in the preparation of biochar, can be beneficial to the improvement of pore properties and the increase of oxygen functional groups [39], therefore in this study, the specific surface area and pore volume of magnetic biochar/Ni composites are remarkable improved, among which, KOH works best in the preparation of wakame biochar. After activation, magnetic biochar/Ni composites possess larger specific surface area and abundant functional groups, endowing them more active sites, which facilitates the binding and adsorption of diesel molecules [40]. Moreover, the well-developed porous structure is also conducive to the adsorption of organic molecules through the capillary effect of the pores. It can be concluded that the best ratio of wakame biochar to activator is 1:0.5, that is, WBPA 0.5, WBHZ 0.5 and WBPH 0.5 have relatively larger specific surface area, thus WBPA 0.5, WBHZ 0.5 and WBPH 0.5 were chosen as adsorbents in the following batch adsorption experiments.

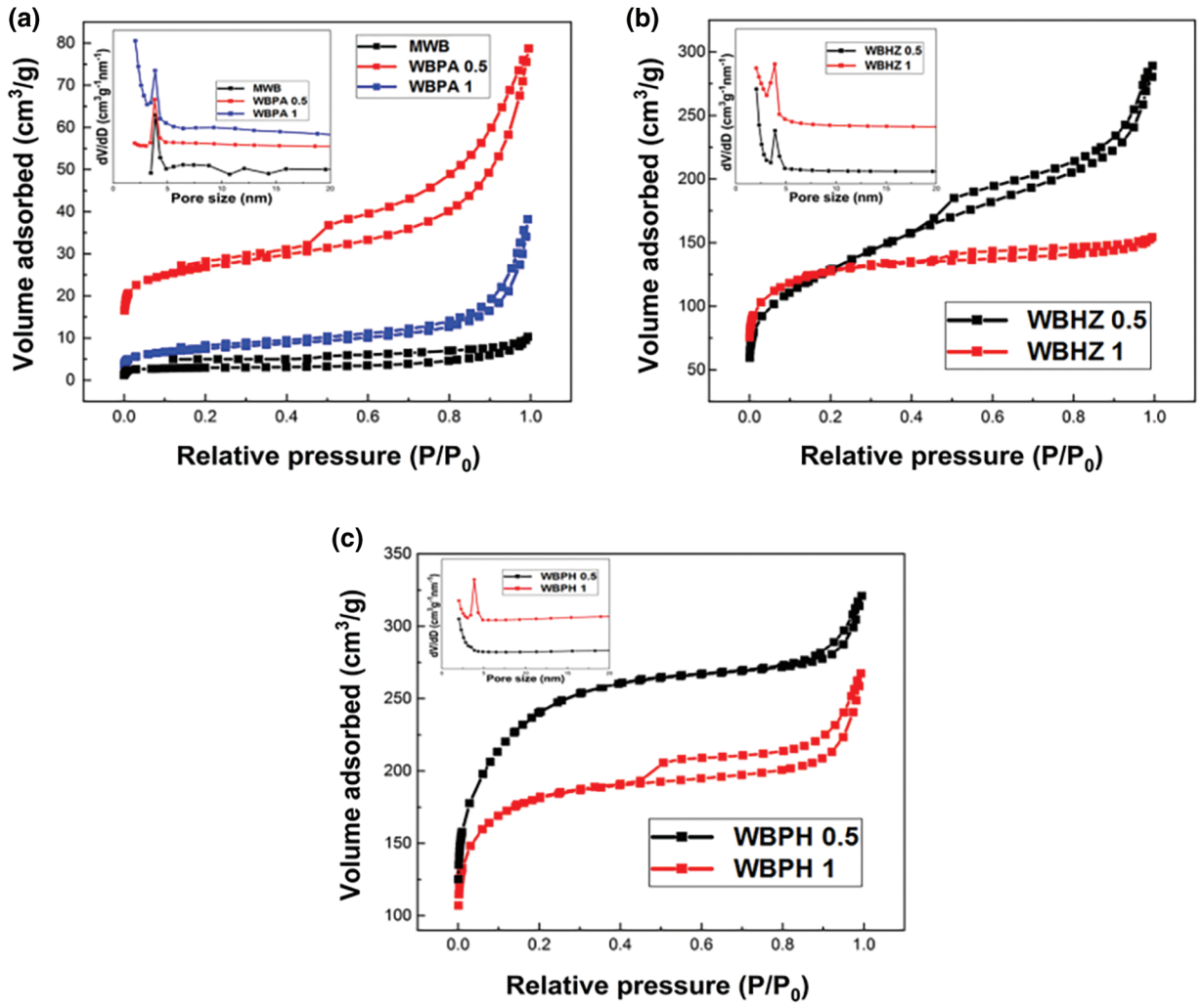


**Figure 1:** $N_2$ adsorption-desorption isotherm and pore size distribution of magnetic Wakame bio-carbon nanocomposite with different activators

**Table 1:** BET parameters of magnetic wakame biochar nanocomposites

| Sample | $S_{BET}$ ($m^2/g$) | $V_{tot}$ ($cm^3/g$) | Average pore diameter (nm) |
|---|---|---|---|
| MWB | 9.151 | 0.011 | 4.787 |
| WBPA 0.5 | 89.501 | 0.092 | 4.119 |
| WBPA 1 | 25.726 | 0.033 | 4.238 |
| WBHZ 0.5 | 455.626 | 0.373 | 2.141 |
| WBHZ 1 | 422.897 | 0.226 | 2.275 |
| WBPH 0.5 | 824.174 | 0.445 | 2.158 |
| WBPH 1 | 601.501 | 0.346 | 2.302 |

*3.1.2 Morphology and Structure Analysis: SEM and TEM*

The morphology and microstructure of the magnetic biochar/Ni composites were analyzed by SEM (Fig. 2). It can be observed that MWB exhibits a relatively dense structure with a small number of holes and cavities. After activation, WBHZ 0.5 and WBPA 0.5 show irregular and fluffy structure with a large number of cavities, cracks and debris, while WBPH 0.5 presents a "honeycomb"-like regular pore structure, which can provide stronger adsorption driving force and more active adsorption sites for diesel adsorption. These carbohydrate polymers are pyrolyzed in the process, dehydration, dehydroxylation, condensation and polymerization form a dense block structure [41], which produces the Ostwald ripening effect, which is the growth of larger particles at the expense of smaller particles. The pores and cavities in the magnetic biochar/Ni composites act as the channels of the active sites, facilitate to bind more diesel molecules. In addition, during the high-temperature pyrolysis process, nickel ions are reduced to metallic nickel embedded in biochar, which have been observed in SEM images of the magnetic biochar/Ni composites, contributing to the separation and recovery of biochar.

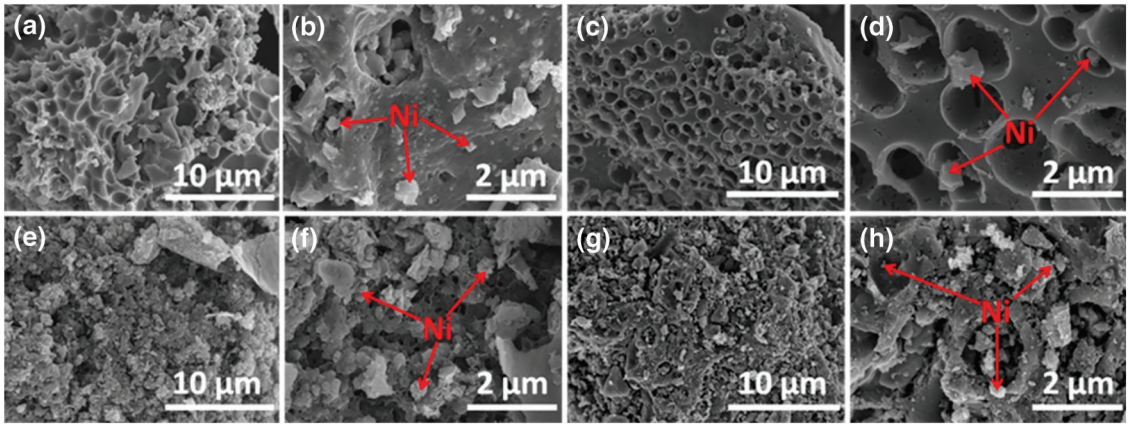


**Figure 2:** SEM image of magnetic Wakame bio-carbon nanocomposite. ((a), (b) are MWB; (c), (d) are WBPH 0.5; (e), (f) are WBHZ 0.5; (g), (h) is WBPA 0.5)

TEM was employed to further analyze the pore structure of the magnetic biochar/Ni composites, it can be seen from TEM images (Fig. 3) that the black dots in the picture may be reduced metal Ni particles, indicating the high uniformity and dispersibility of Ni particles on the magnetic wakame bio-carbon nanocomposite. The surface of the magnetic wakame bio-carbon nanocomposite material activated by the activation reagent has a layered structure, which is sponge-like and has irregular pores, indicating that there are a large number of uniform micropores. A large number of dense concave-convex pores indicate that the pores have been enriched after the activated magnetic biochar.

*3.1.3 Analysis of Chemical Composition and Crystal Structure*

According to the FTIR spectrum (Fig. 4a) of magnetic biochar/Ni composites, it can be observed that there is a slight change before and after activation of magnetic biochar/Ni composites. There is a broad band around 3400 $cm^{-1}$ is the -OH stretching band of the alcohol or phenol group [42]. Due to the stretching vibration of the aliphatic -CH group, a characteristic band appears near 2910 $cm^{-1}$, due to the primary amine (NH) group Vibration, the characteristic band appears near 1586 $cm^{-1}$. In addition, the peaks appearing at 1400–1440 $cm^{-1}$ can be attributed to the vibration of the $-CH_2$ and $-CH_3$ groups [43], while the C-O of alcohols, carboxylic acids and ethers the stretching vibration shows a broadband in the range of 1050–1210 $cm^{-1}$, because during the pyrolysis process, different forms of oxygen in the macroalgae are converted into carbon-oxygen bonds in the form of bond chains. However, the out-of-plane curvature of =C-H on the aromatic ring shows low-intensity vibration near 879 $cm^{-1}$, and the presence of a large number of organic active groups (such as -OH, -NH and -CH) help the adsorbent to dye dyes.

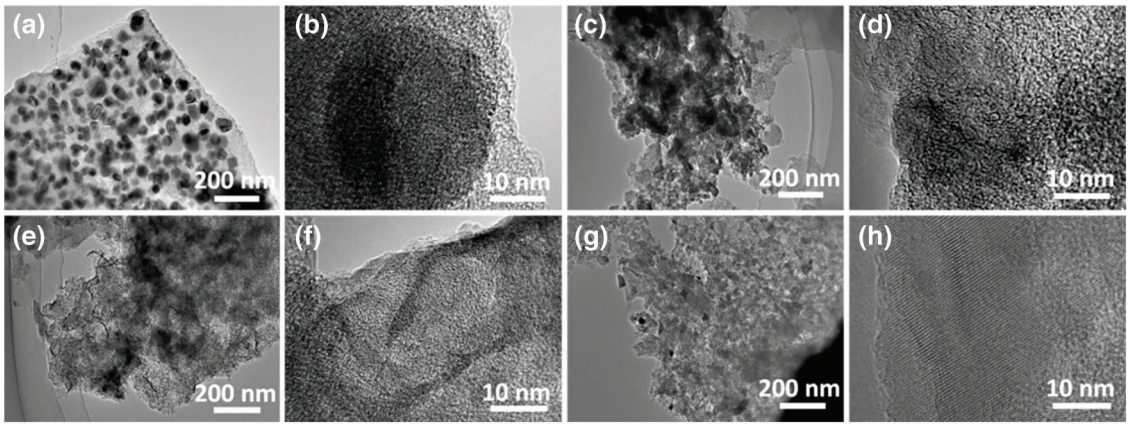


**Figure 3:** TEM image of magnetic wakame bio-carbon nanocomposite ((a), (b) are MWB; (c), (d) are WBPH 0.5; (e), (f) are WBHZ 0.5; (g), (h) is WBPA 0.5)

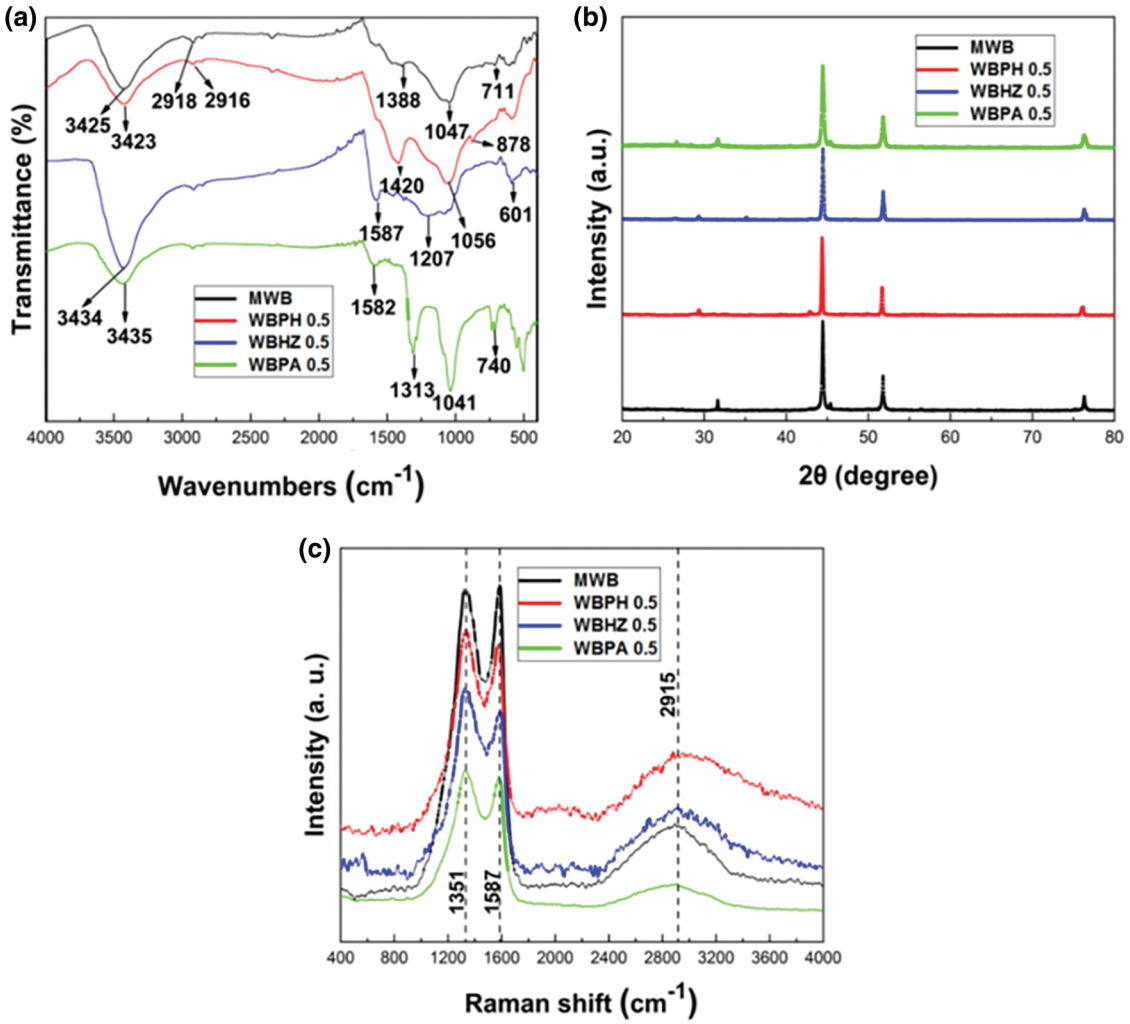


**Figure 4:** Chemical composition and crystal structure analysis diagram ((a) is FTIR, (b) is XRD, (c) is Raman spectrum)

The XRD pattern (Fig. 4b) of the magnetic biochar/Ni composites shows that the diffraction peak intensity of WBPA 0.5, WBHZ 0.5 and WBPH 0.5 is higher than that of MWB. This is because the activation reagent consumes part of the carbon element for pore formation. As a result, the metal Ni content increases, and the diffraction peaks are mainly concentrated between 40° and 80°. 2θ = 44.480°, 51.830° and 76.350° diffraction peaks correspond to (1,1,1), (2,0,0), (2,2,0) element nickel [44], thus It proves that the metal Ni is successfully loaded onto the wakame magnetic biochar composite material. The existence of metal Ni makes it possible to conveniently recover the adsorbent material for recycling after the end of the adsorption experiment.

The Raman spectrum (Fig. 4c) of magnetic biochar/Ni composites have been obtained to investigate their graphitization state. There are three peaks located at 1351 $cm^{-1}$, 1587 $cm^{-1}$ and 2915 $cm^{-1}$, corresponding to the D, G and 2D band, respectively. The D band corresponds to $sp^3$ hybridized carbon in disordered state, the G band is related to the vibration of $sp^2$-hybridized carbon atoms in a graphitic layer [45], and the 2D band is attributed to the double resonant Raman scattering with two-phonon emissions [46]. The intensity ratio of the D and the G-band ($I_D/I_G$) is a measure of the disorder of as-prepared samples [47]. Compared to the $I_D/I_G$ ratio of MWB (0.89), that of WBPA 0.5, WBHZ 0.5 and WBPH 0.5 are 1.05, 1.07 and 1.03, respectively, indicating that a large number of disordered carbons were contained in MWB, while WBPA 0.5, WBHZ 0.5 and WBPH 0.5 are relatively less, due to partial carbon being consumed during high temperature activation, which is consist with the results of elemental analysis.

*3.1.4 Elemental Analysis and ICP Determination*

Elemental analyzer and ICP-OES were employed to investigate the main components of the magnetic biochar/Ni composites, as illustrated in Table 2. It can be obviously seen that the carbon content of WBPH 0.5 (39.13%), WBHZ 0.5 (42.05%) and WBPA 0.5 (43.61%) are lower than that of MWB (51.98%), attributed to the consumption of some carbon elements during the activation process. As usual, the lower the O/C atomic ratio, the higher the hydrophobicity of biochar materials, and WBPA 0.5 has a lowest O/C ratio (0.151), indicating that it is more hydrophobic. The polar index (O+N)/C atomic ratio of WBPH 0.5, WBHZ 0.5 and WBPA 0.5 reflects the existence of polar groups in the magnetic wakame bio-carbon nanocomposite [48]. The H/C atomic ratio is usually used to estimate the aromaticity of biochar [49]. The H/C atomic ratios of WBPH 0.5, WBHZ 0.5 and WBPA 0.5 decreased by 0.334, 0.242 and 0.292, respectively, which indicates that the addition of activator increases the aromaticity of biochar. These features are conducive to the adsorption of diesel organic macromolecules.

**Table 2:** Elemental analysis of magnetic wakame biochar nanocomposites (mass, %)

| Element | C | H | N | O | S | O/C | (O+N)/C | H/C | Ni |
|---|---|---|---|---|---|---|---|---|---|
| MWB | 51.98 | 2.47 | 2.03 | 11.28 | 0.64 | 0.163 | 0.196 | 0.570 | 28.69 |
| WBPH 0.5 | 39.13 | 0.77 | 1.58 | 13.37 | 0.14 | 0.256 | 0.291 | 0.236 | 29.57 |
| WBHZ 0.5 | 42.05 | 1.15 | 2.81 | 9.98 | 1.26 | 0.178 | 0.235 | 0.328 | 33.70 |
| WBPA 0.5 | 43.61 | 1.01 | 0.45 | 8.79 | 0.24 | 0.151 | 0.160 | 0.278 | 37.64 |

Besides, the nickel contents of as-prepared samples have been analyzed by ICP-OES, compared with the nickel content of MWB, those of the magnetic biochar/Ni composites increase remarkably, among which, that of WBPA 0.5 is maximum (37.64%). The loading of nickel could contribute to the separation and recovery of the magnetic biochar/Ni composites after adsorption.

### *3.2 Batch Adsorption Experiments*

#### *3.2.1 Effects of Different Adsorbents on Diesel Adsorption*

The adsorption performances for diesel using seven different adsorbents (MWB, WBPA 0.5, WBPA 1, WBHZ 0.5, WBHZ 1, WBPH 0.5 and WBPH 1) have been investigated, as shown in Fig. 5. It can be observed that the adsorption capacities of the magnetic biochar/Ni composites rise sharply after activation, among which, those of WBPH are highest, followed by WBHZ and WBPA. As the ratio of activator increases, the adsorption capacities of diesel using the magnetic biochar/Ni composites decrease, which may be due to the collapse of the pore size caused by the excessive addition of activator in the process of high-temperature pore formation, resulting in a small specific surface area and reduced adsorption. And the adsorption capacity of diesel using WBPA 0.5, WBHZ 0.5 and WBPH 0.5 are 3.92, 7.75 and 9.75 g/g, respectively. At the initial stage of adsorption, the adsorption capacities of diesel using the magnetic biochar/Ni composites increase sharply, and the adsorption equilibrium is reached in about 20 min, because there is abundant porous structure, high specific surface area and various functional groups of the magnetic biochar/Ni composites at the beginning of adsorption reaction, rendering them plenty of active sites and adsorbing diesel molecules quickly, while as the reaction continues, more and more active sites are occupied, the adsorption capacity decreases until adsorption equilibrium.

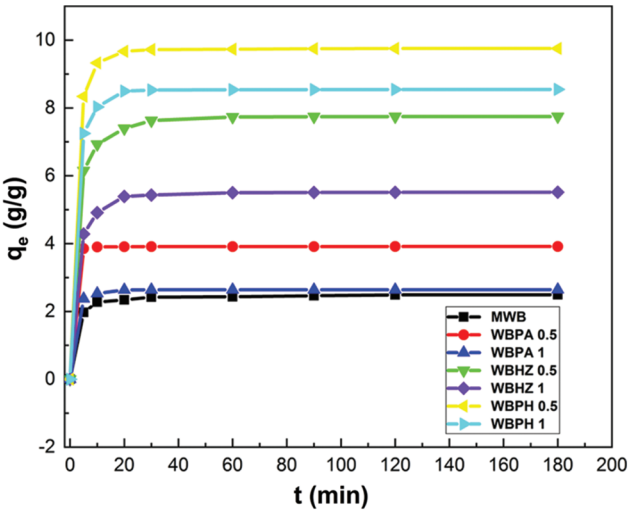


**Figure 5:** The adsorption performance of seven different adsorbents for diesel

#### *3.2.2 Effects of Diesel Initial Concentrations on Diesel Adsorption*

Fig. 6 shows that the adsorption capacities of diesel using WBPA 0.5, WBHZ 0.5 and WBPH 0.5 increase as the diesel initial concentration increases, among which, the adsorption capacity of diesel using WBPH 0.5 at 10 mL diesel concentration is highest, up to 13.476 g/g. Moreover, as the diesel initial concentration increases, the time to reach equilibrium of the diesel adsorption using the magnetic biochar/Ni composites is shorter, which can be attributed to more active sites exposed on their surface being available for the adsorption of diesel. And in the initial reaction period, the adsorption rate of diesel using the magnetic biochar/Ni composites are quite fast, and the adsorption system of diesel using WBPA 0.5 can quickly reach equilibrium, while those of WBHZ 0.5 and WBPH 0.5 take a relatively long time to reach equilibrium. As the adsorption processes, the adsorption rate of diesel using the magnetic biochar/Ni composites gradually decrease and flat out, attributable to vast active sites being occupied by diesel molecules, leading to competitive adsorption and lower the attractiveness to diesel molecules [50].

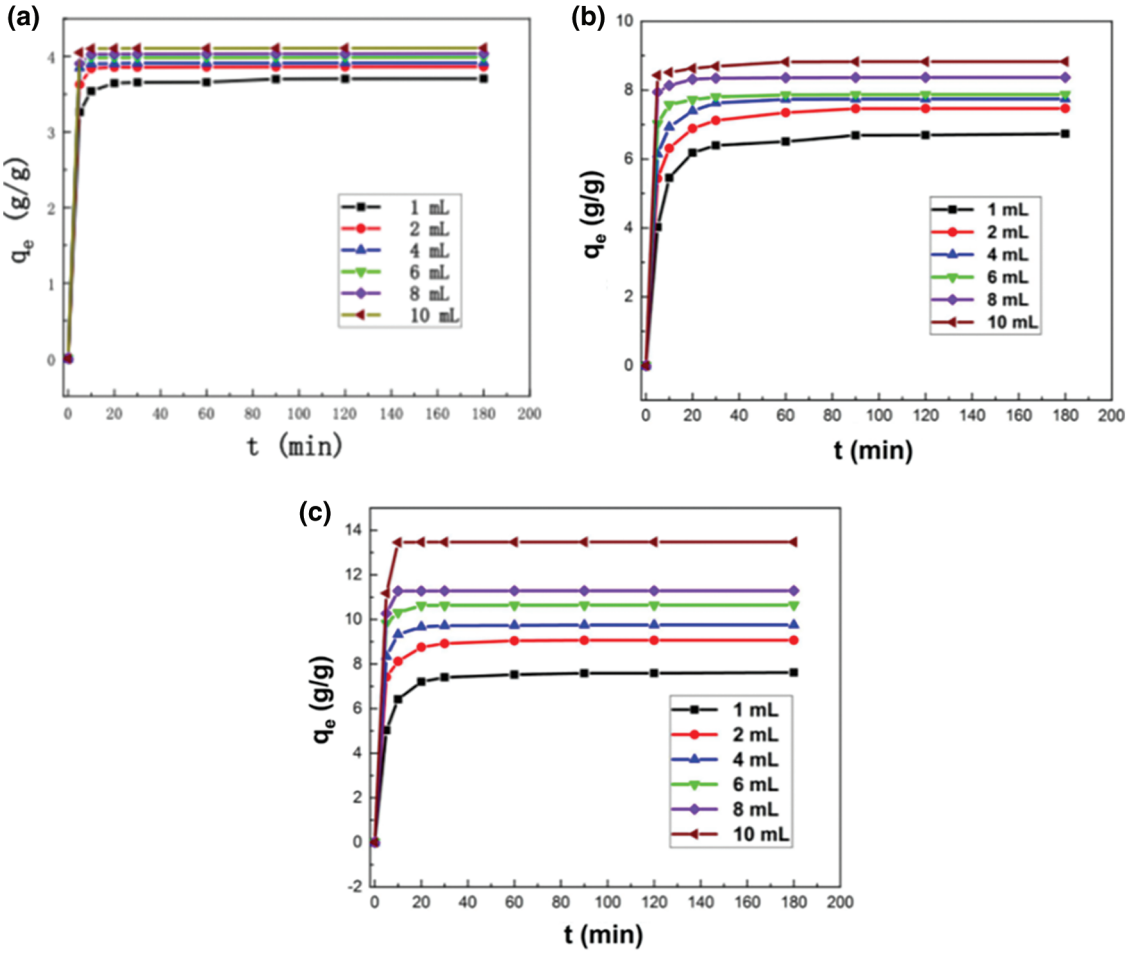


**Figure 6:** The adsorption performances of diesel using the magnetic biochar/Ni composites (a: WBPA 0.5, b: WBHZ 0.5, c: WBPH 0.5) at different diesel initial concentration (1, 2, 4, 6, 8 and 10 mL) in the range from 0 min to 180 min

### *3.3 Adsorption Isotherms and Kinetics Studies*

#### *3.3.1 Adsorption Isotherms Studies*

The effects of adsorbent dosage on diesel adsorption using WBPH 0.5, WBPA 0.5 and WBHZ 0.5 have been analyzed, as shown in Fig. 7. It can be observed that the removal efficiency of diesel using the magnetic biochar/Ni composites remarkably rises and then levels off with the increase of adsorbent dosage in the range of 0.1–0.7 g, due to the availability of more active sites on their surface [51]. And the removal efficiency of diesel using WBHZ 0.5 is the highest, up to 100%, followed by WBPA 0.5 is 99.74%, and WBPH 0.5 is 46.55%. Therefore, considering the removal efficiency and practicability, the optimum adsorbent dosage is selected to be 0.6 g for diesel adsorption.

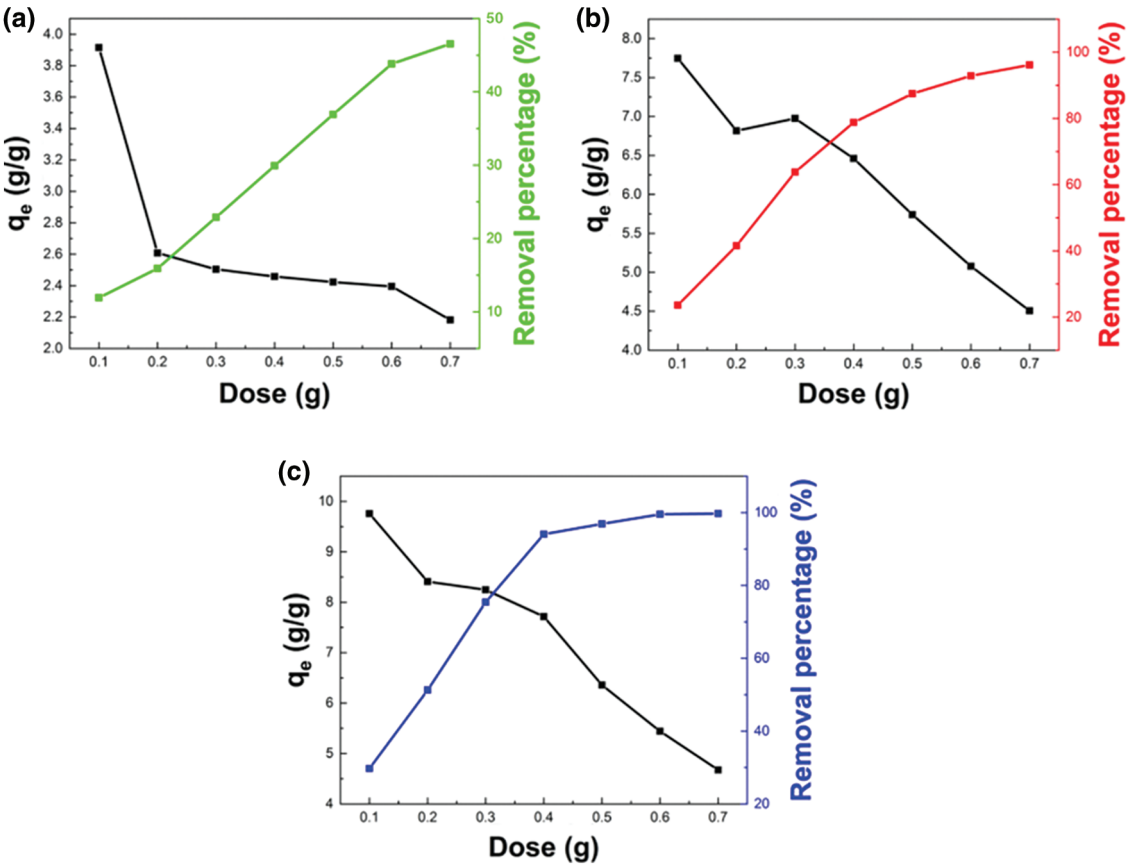


**Figure 7:** The effect of WBPH 0.5 (a), WBPA 0.5 (b) and WBHZ 0.5 (c) adsorbent dosage on diesel adsorption

*3.3.2 Adsorption Kinetics Studies*

In order to study adsorption equilibrium, adsorption isotherm model was chosen according to the properties and types of the system. The most commonly used models are Langmuir Eq. (2) and Freundlich Eq. (3).

$$\frac{C_e}{q_e} = \frac{C_e}{q_L} + \frac{1}{K_L q_L} \tag{2}$$

$$q_e = K_F C_e^{1/n} \tag{3}$$

where $C_e$ (g/L) represents concentration of diesel at equilibrium, $q_e$ (g/g) and $q_L$ (g/g) are adsorption capacity of diesel at equilibrium and saturation, respectively. $K_L$ (L/mg) is the Langmuir adsorption equilibrium constant, $K_F$ [(g/g) (L/g) 1/n] is the Freundlich constant, and 1/n is the adsorption intensity factor or surface heterogeneity.

In order to study the diesel adsorption using the magnetic biochar/Ni composites, the traditional Langmuir and Freundlich adsorption isotherm models are employed to analyze the adsorption isotherms. Fig. 8 indicates the fitting of data with isotherm models, and adsorption parameters and regression data of the models are presented in Table 3. It can be demonstrated that Regression coefficient ($R^2$) of Langmuir model has higher value (0.999, 0.994 and 0.964) for the diesel adsorption using WBPA 0.5, WBHZ 0.5 and WBPH 0.5, indicating that Langmuir equation is more suitable for describing the diesel

adsorption using the magnetic biochar/Ni composites, and their adsorption processes are monolayer adsorption [52]. The calculated adsorption amount of diesel using WBPA 0.5, WBHZ 0.5 and WBPH 0.5 at equilibrium is 4.13, 8.79, and 13.05 g/g, respectively, which are in good combination with experimental data, i.e., the experimental value is 4.11, 8.83 and 13.47 g/g, respectively. Compared with the previous biochar removal of diesel fuel [53], the magnetic biochar/Ni composites have good adsorption capacity values for diesel.

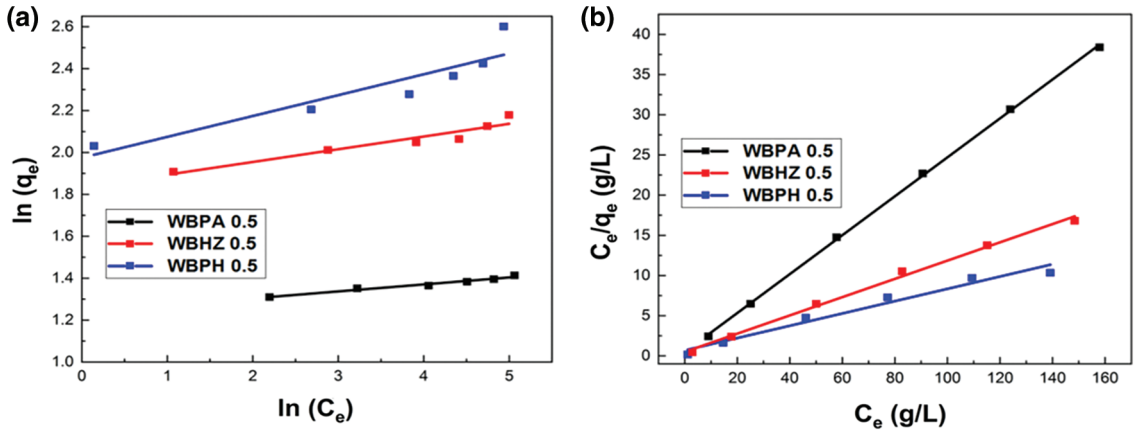


**Figure 8:** The Freundlich (a) and Langmuir (b) adsorption isotherm models

**Table 3:** Parameters of the adsorption isotherm model

| Adsorbent | Freundlich | | | Langmuir | | |
|---|---|---|---|---|---|---|
| | n | $K_F$ [(g/g)(L/g)$^{1/n}$] | $R^2$ | $q_L$(g/g) | $K_L$(L/g) | $R^2$ |
| WBPA 0.5 | 30.05 | 3.45 | 0.965 | 4.13 | 0.481 | 0.999 |
| WBHZ 0.5 | 16.47 | 6.25 | 0.892 | 8.79 | 0.231 | 0.994 |
| WBPH 0.5 | 10.04 | 7.21 | 0.806 | 13.05 | 0.113 | 0.964 |

*3.3.3 Adsorption Kinetics Studies*

In order to further study the adsorption kinetics of the mixed system, the pseudo-first-order model Eq. (4), pseudo-second-order model Eq. (5) and the intraparticle diffusion model Eq. (6) are used for analysis and evaluation.

$$\ln(q_e - q_t) = \ln q_e - k_1 t \tag{4}$$

$$\frac{t}{q_t} = \frac{1}{k_2 q_e^2} + \frac{t}{q_e} \tag{5}$$

$$q_t = k_{di} t^{1/2} + C_i \tag{6}$$

where $q_e$ (g/g) and $q_t$ (g/g) are the adsorption amount of diesel at equilibrium and at time t (min), respectively. $k_1$ (min$^{-1}$) and $k_2$ (g/g min) are the rate constant of the PFO and PSO, respectively. $k_{di}$ (g/g·min$^{1/2}$) is intraparticle diffusion model constant. $C_i$ (g/g) is boundary layer thickness constant and t (min) is time.

Adsorption kinetic as a key factor determines the uptake rate of solute, representing the adsorption efficiency of adsorbent. Pseudo-first-order (PFO), Pseudo-second-order (PSO), and Weber-Morris

intraparticle diffusion model were applied for the kinetics model fitting of diesel adsorption data. Fig. 9 indicates the fitting of experimental data with the three kinetics models for diesel adsorption, and Table 4 provides the results of the PFO and PSO kinetics models fittings for diesel adsorption using the magnetic biochar/Ni composites. It can be demonstrated that the $R^2$ value in the PSO model of diesel adsorption using WBPA 0.5, WBHZ 0.5 and WBPH 0.5 is all 0.999, higher than that in the PFO model, indicating that the PSO model could better describe the adsorption of diesel using the magnetic biochar/Ni composites, being used to calculate the adsorption amounts of diesel at equilibrium is in good combination with experimental data. As is well known, the PSO equation model belongs to chemical adsorption, which means that chemical reaction is also involved in diesel adsorption process using the magnetic biochar/Ni composites [54].

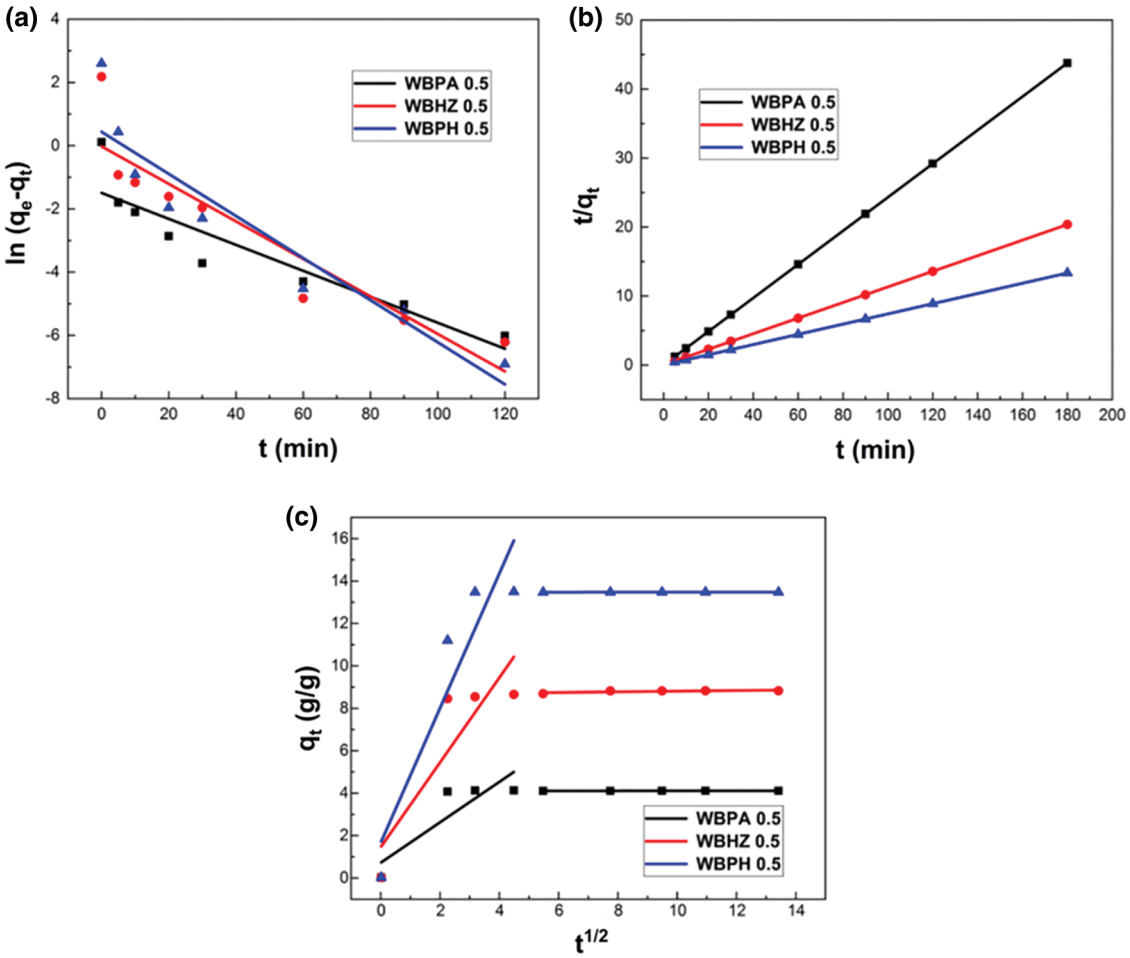


**Figure 9:** The Pseudo-first-order (a), Pseudo-second-order (b), and Weber-Morris intraparticle diffusion (c) model

**Table 4:** The adsorption kinetic parameters of diesel using WBPA 0.5, WBHZ 0.5 and WBPH 0.5 in the PFO and PSO model

| Adsorbent | $q_{e,exp}$ (g/g) | Pseudo-first order | | | Pseudo-second order | | |
|---|---|---|---|---|---|---|---|
| | | $q_{e,cal}$ (g/g) | $k_1$ ($min^{-1}$) | $R^2$ | $q_{e,cal}$ (g/g) | $k_2$ (g $g^{-1}$ $min^{-1}$) | $R^2$ |
| WBPA 0.5 | 4.11 | 0.22 | 0.041 | 0.817 | 4.11 | 4.172 | 0.999 |
| WBHZ 0.5 | 8.83 | 0.98 | 0.059 | 0.829 | 8.85 | 0.114 | 0.999 |
| WBPH 0.5 | 13.47 | 1.55 | 0.067 | 0.856 | 13.51 | 0.074 | 0.999 |

In order to analyze the control step of diesel adsorption process, the adsorption kinetics of the magnetic biochar/Ni composites for diesel are investigated by the Weber-Morris intraparticle diffusion model, as shown in Fig. 9c. The intraparticle diffusion parameters of diesel adsorption using WBPA 0.5, WBHZ 0.5 and WBPH 0.5 are shown in Table 5. It can be noted that the fitting of data using intraparticle diffusion model is linear but does not pass through the origin, so intraparticle diffusion is not a sole rate controlling adsorption process. Fig. 9c shows the intraparticle diffusion model has dual-linear characteristics between qt and $t^{1/2}$, indicating that the diesel adsorption using the magnetic biochar/Ni composites can be considered as a two-step process, among which, the first step rises sharply, being regarded as the outer-surface adsorption of the magnetic biochar/Ni composites, while the second step tends towards equilibrium, whose rate is limited by the intra-particle diffusion of particles. A larger slope can be observed from the first sharp section, indicating a higher removal rate of diesel oil, which can be attributed to the macroscopic structure of the magnetic wakame biochar composite material is closer to the microporous "honeycomb" structure than the macroporous "capillary" structure, and the "honeycomb" structure can provide stronger adsorption driving force and more active adsorption sites [55]. The slope of the second section is lower than that of the first section. This may be due to the slow diffusion of diesel molecules in the magnetic wakame bio-carbon nanocomposite material, resulting in a low removal rate, mainly due to the decrease of the micropore density gradient. The two-stage continuous mass transfer corresponds to the external to internal mass transfer and intra-particle diffusion in the pore and microporous structure of the magnetic wakame bio-carbon nanocomposite.

**Table 5:** Intraparticle diffusion model

| Adsorbent | Intraparticle diffusion | | | | | |
|---|---|---|---|---|---|---|
| | $k_{d1}$ (g/g $min^{1/2}$) | $C_1$(g/g) | $R_1^2$ | $k_{d2}$(g/g $min^{1/2}$)× $10^{-3}$ | $C_2$(g/g) | $R_2^2$ |
| WBPA 0.5 | 0.953 | 0.714 | 0.755 | 0.781 | 4.101 | 0.951 |
| WBHZ 0.5 | 1.997 | 1.465 | 0.768 | 0.714 | 8.652 | 0.943 |
| WBPH 0.5 | 3.172 | 1.699 | 0.891 | 0.673 | 13.467 | 0.956 |

Therefore, in addition to the intra-particle diffusion resistance, the adsorption mechanism of the system is also affected. In addition, it was observed from the FTIR spectrum that the functional groups (such as -OH, -NH and -CH) in the magnetic wakame biochar composite material have the effect of promoting the binding of diesel molecules to the active sites on the surface of the material. BET shows that high specific surface area and rich pore structure help to improve mass transfer efficiency.

### *3.4 Magnetic Recovery Cycle Experiment*

The magnetic wakame bio-carbon nanocomposite material can be separated from water under the action of an external magnetic field. The key to the sustainable application of this type of magnetic biochar is its reusability and good stability. The magnetic properties of WBPA 0.5, WBHZ 0.5 and WBPH 0.5 were measured using the VSM technique under a magnetic field between −20,000 Oe and 20,000 Oe, as shown in Fig. 10, the saturated magnetization (Ms) of the WBPA 0.5 reaches up to 102.47 emu $g^{-1}$, exhibiting good magnetic separation performance. After the five times recycling of adsorption and desorption, the adsorption capacity of WBPA 0.5, WBHZ 0.5 and WBPH 0.5 for diesel only decreased by 3.16%, 7.27% and 9.28%, respectively (Fig. 11), demonstrating their good cycle stability and reusability. Therefore, the magnetic wakame biochar composite material has great potential in actual industrial wastewater treatment.

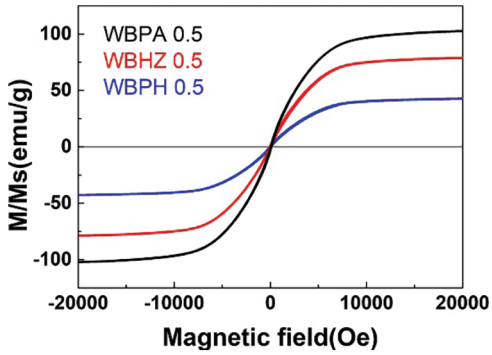


**Figure 10:** Magnetization curve of WBPA 0.5, WBHZ 0.5 and WBPH 0.5

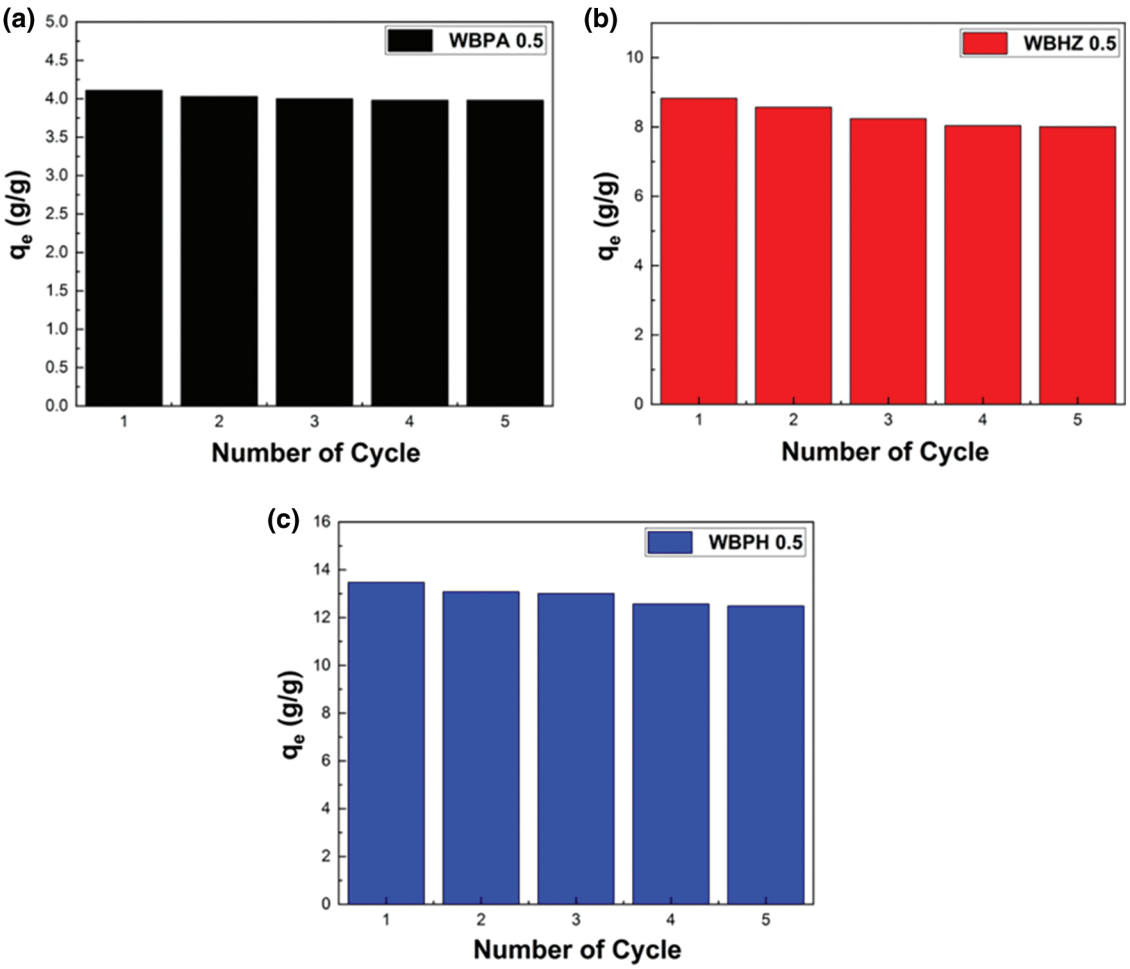


**Figure 11:** The reusability of magnetic wakame biochar composites

## 4 Conclusions

The magnetic wakame biochar/Ni composites were prepared with different activating reagents, which have larger specific surface area, abundant porous structure, and various reactive groups, endowing them with superior adsorption performance. The maximum adsorption capacities for diesel using WBPA 0.5,

WBHZ 0.5 and WBPH 0.5 are 4.11, 8.83, and 13.47 g/g, respectively. The adsorption process is more suitable for the Langmuir model and the Pseudo-second-order model. After five adsorption-desorption cycles, the biochar/Ni composites still have higher adsorption efficiency, exhibiting good stability and reusability. Therefore, the magnetic wakame biochar/Ni composites are expected to become potential adsorbents for the treatment of oily wastewater.

**Acknowledgement:** This study was supported by the Fundamental Research Funds for Zhejiang Provincial Universities and Research Institutes (No. 2021J004), the National Natural Science Foundation of China (U1809214), and the Natural Science Foundation of Zhejiang Province (LY20E080014).

**Funding Statement:** The authors received no specific funding for this study.

**Conflicts of Interest:** The authors declare that they have no conflicts of interest to report regarding the present study.

## References

1. Bandura, L., Franus, M., Józefaciuk, G., Franus, W. (2015). Synthetic zeolites from fly ash as effective mineral sorbents for land-based petroleum spills cleanup. *Fuel, 147,* 100–107. DOI 10.1016/j.fuel.2015.01.067.
2. Osin, O. A., Yu, T., Lin, S. (2017). Oil refinery wastewater treatment in the Niger Delta, Nigeria: Current practices, challenges, and recommendations. *Environmental Science and Pollution Research, 24(28),* 22730–22740. DOI 10.1007/s11356-017-0009-z.
3. Dubansky, B., Whitehead, A., Miller, J. T., Rice, C. D., Galvez, F. (2013). Multitissue molecular, genomic, and developmental effects of the Deepwater Horizon oil spill on resident Gulf killifish (*Fundulus grandis*). *Environmental Science & Technology, 47(10),* 5074–5082. DOI 10.1021/es400458p.
4. Hu, Y., Zhu, Y., Wang, H., Wang, C., Li, H. et al. (2017). Facile preparation of superhydrophobic metal foam for durable and high efficient continuous oil-water separation. *Chemical Engineering Journal, 322,* 157–166. DOI 10.1016/j.cej.2017.04.034.
5. Zhou, X., Zhang, Z., Xu, X., Men, X., Zhu, X. (2013). Facile fabrication of superhydrophobic sponge with selective absorption and collection of oil from water. *Industrial & Engineering Chemistry Research, 52(27),* 9411–9416. DOI 10.1021/ie400942t.
6. Stout, S. A., Payne, J. R. (2016). Chemical composition of floating and sunken *in-situ* burn residues from the *Deepwater Horizon* oil spill. *Marine Pollution Bulletin, 108(1–2),* 186–202. DOI 10.1016/j.marpolbul.2016.04.031.
7. Bagby, S. C., Reddy, C. M., Aeppli, C., Fisher, G. B., Valentine, D. L. (2017). Persistence and biodegradation of oil at the ocean floor following Deepwater Horizon. *Proceedings of the National Academy of Sciences of the United States of America, 114(1),* E9–E18. DOI 10.1073/pnas.1610110114.
8. Del'Arco, J., de Franca, F. (2001). Influence of oil contamination levels on hydrocarbon biodegradation in sandy sediment. *Environmental Pollution, 112(3),* 515–519. DOI 10.1016/S0269-7491(00)00128-7.
9. Liu, L., Wang, L., Song, W., Yang, L., Yin, L. et al. (2018). Crude oil removal from aqueous solution using raw and carbonized Xanthoceras sorbifolia shells. *Environmental Science and Pollution Research, 25(29),* 29325–29334. DOI 10.1007/s11356-018-2895-0.
10. D'Andrea, M. A., Reddy, G. K. (2018). The development of long-term adverse health effects in oil spill cleanup workers of the Deepwater Horizon offshore drilling rig disaster. *Frontiers in Public Health, 6,* 117. DOI 10.3389/fpubh.2018.00117.
11. Ferguson, A., Solo-Gabriele, H., Mena, K. (2020). Assessment for oil spill chemicals: Current knowledge, data gaps, and uncertainties addressing human physical health risk. *Marine Pollution Bulletin, 150(3),* 110746. DOI 10.1016/j.marpolbul.2019.110746.
12. Doshi, B., Sillanpää, M., Kalliola, S. (2018). A review of bio-based materials for oil spill treatment. *Water Research, 135(8S),* 262–277. DOI 10.1016/j.watres.2018.02.034.

13. Banerjee, S. S., Joshi, M. V., Jayaram, R. V. (2006). Treatment of oil spill by sorption technique using fatty acid grafted sawdust. *Chemosphere, 64(6),* 1026–1031. DOI 10.1016/j.chemosphere.2006.01.065.
14. Jin, J., Wang, H., Jing, Y., Liu, M., Wang, D. et al. (2019). An efficient and environmental-friendly dispersant based on the synergy of amphiphilic surfactants for oil spill remediation. *Chemosphere, 215,* 241–247. DOI 10.1016/j.chemosphere.2018.09.159.
15. Abtahi, H., Parhamfar, M., Saeedi, R., Villasenor, J., Sartaj, M. et al. (2020). Effect of competition between petroleum-degrading bacteria and indigenous compost microorganisms on the efficiency of petroleum sludge bioremediation: Field application of mineral-based culture in the composting process. *Journal of Environmental Management, 258(1),* 110013. DOI 10.1016/j.jenvman.2019.110013.
16. Rahmani, Z., Rashidi, A. M., Samadi, M. T., Rahmani, A. R. (2018). N-doped reduced graphene oxide aerogel for the selective adsorption of oil pollutants from water: Isotherm and kinetic study. *Journal of Industrial and Engineering Chemistry, 61,* 416–426. DOI 10.1016/j.jiec.2017.12.041.
17. Robati, D., Mirza, B., Rajabi, M., Moradi, O., Tyagi, I. et al. (2016). Removal of hazardous dyes-BR 12 and methyl orange using graphene oxide as an adsorbent from aqueous phase. *Chemical Engineering Journal, 284(17),* 687–697. DOI 10.1016/j.cej.2015.08.131.
18. Okiel, K., Sayed, M., Kady, M. Y. (2011). Treatment of oil-water emulsions by adsorption onto activated carbon, bentonite and deposited carbon. *Egyptian Journal of Petroleum, 20(2),* 9–15. DOI 10.1016/j.ejpe.2011.06.002.
19. Moazed, H., Viraraghavan, T. (2005). Removal of oil from water by bentonite organoclay. *Practice Periodical of Hazardous, Toxic, and Radioactive Waste Management, 9(2),* 130–134. DOI 10.1061/(ASCE)1090-025X(2005)9:2(130).
20. Wang, D., Mclaughlin, E., Pfeffer, R., Lin, Y. (2012). Adsorption of oils from pure liquid and oil-water emulsion on hydrophobic silica aerogels. *Separation and Purification Technology, 99,* 28–35. DOI 10.1016/j.seppur.2012.08.001.
21. Xiaobing, L., Zhang, C., Jiongtian, L. (2010). Adsorption of oil from waste water by coal: Characteristics and mechanism. *Mining Science and Technology (China), 20(5),* 778–781. DOI 10.1016/S1674-5264(09)60280-5.
22. Sohi, S. P. (2012). Carbon storage with benefits. *Science, 338(6110),* 1034–1035. DOI 10.1126/science.1225987.
23. Yang, D. P., Li, Z., Liu, M., Zhang, X., Chen, Y. et al. (2019a). Biomass-derived carbonaceous materials: Recent progress in synthetic approaches, advantages, and applications. *ACS Sustainable Chemistry & Engineering, 7(5),* 4564–4585. DOI 10.1021/acssuschemeng.8b06030.
24. Wang, B., Li, M., Zhang, H., Zhu, J., Chen, S. et al. (2020). Effect of straw-derived dissolved organic matter on the adsorption of sulfamethoxazole to purple paddy soils. *Ecotoxicology and Environmental Safety, 203(24),* 110990. DOI 10.1016/j.ecoenv.2020.110990.
25. Rouzitalab, Z., Maklavany, D. M., Jafarinejad, S., Rashidi, A. (2020). Lignocellulose-based adsorbents: A spotlight review of the effective parameters on carbon dioxide capture process. *Chemosphere, 246,* 125756. DOI 10.1016/j.chemosphere.2019.125756.
26. Jiang, X., Wang, H., Hu, E., Lei, Z., Fan, B. et al. (2020). Efficient adsorption of uranium from aqueous solutions by microalgae based aerogel. *Microporous and Mesoporous Materials, 305(3),* 110383. DOI 10.1016/j.micromeso.2020.110383.
27. Zhou, Y., Cai, L., Guo, J., Wang, Y., Ji, L. et al. (2018). Preparation of $Bi_2MoO_6$/kelp biochar nanocomposite for enhancing degradability of methylene blue. *Applied Ecology and Environmental Research, 16(5),* 5837–5847. DOI 10.15666/aeer/1605_58375847.
28. Wu, Y., Chen, Z., Liu, Y., Xu, Y., Liu, Z. (2018). One step synthesis of N-doped activated carbons derived from sustainable microalgae-NaAlg composites for $CO_2$ and $CH_4$ adsorption. *Fuel, 233(11),* 574–581. DOI 10.1016/j.fuel.2018.06.094.
29. Hei, Y., Li, X., Zhou, X., Liu, J., Sun, M. et al. (2018). Electrochemical sensing platform based on kelp-derived hierarchical meso-macroporous carbons. *Analytica Chimica Acta, 1003,* 16–25. DOI 10.1016/j.aca.2017.12.007.
30. Kwon, K. M., Kim, I. G., Lee, K. Y., Kim, H., Kim, M. S. et al. (2019). $\alpha$-$Fe_2O_3$ anchored on porous N doped carbon derived from green microalgae via spray pyrolysis as anode materials for lithium ion batteries. *Journal of Industrial and Engineering Chemistry, 69,* 39–47. DOI 10.1016/j.jiec.2018.09.004.

31. Tan, X. F., Liu, S. B., Liu, Y. G., Gu, Y. I., Zeng, G. M. et al. (2017). Biochar as potential sustainable precursors for activated carbon production: Multiple applications in environmental protection and energy storage. *Bioresource Technology, 227(1),* 359–372. DOI 10.1016/j.biortech.2016.12.083.
32. Sizmur, T., Fresno, T., Akgül, G., Frost, H., Jiménez, E. (2017). Biochar modification to enhance sorption of inorganics from water. *Bioresource Technology, 246(5),* 34–47. DOI 10.1016/j.biortech.2017.07.082.
33. Angın, D., Altintig, E., Köse, T. E. (2013). Influence of process parameters on the surface and chemical properties of activated carbon obtained from biochar by chemical activation. *Bioresource Technology, 148,* 542–549. DOI 10.1016/j.biortech.2013.08.164.
34. Ho, S. H., Wang, D., Wei, Z. S., Chang, J. S., Ren, N. Q. (2018). Lead removal by a magnetic biochar derived from persulfate-ZVI treated sludge together with one-pot pyrolysis. *Bioresource Technology, 247(8),* 463–470. DOI 10.1016/j.biortech.2017.09.125.
35. Zhang, S., Ji, Y., Dang, J., Zhao, J., Chen, S. (2019). Magnetic apple pomace biochar: Simple preparation, characterization, and application for enriching Ag(I) in effluents. *Science of the Total Environment, 668,* 115–123. DOI 10.1016/j.scitotenv.2019.02.318.
36. Yao, X., Ji, L., Guo, J., Ge, S., Lu, W. et al. (2020). Magnetic activated biochar nanocomposites derived from wakame and its application in methylene blue adsorption. *Bioresource Technology, 302(3),* 122842. DOI 10.1016/j.biortech.2020.122842.
37. Scheufele, F. B., Módenes, A. N., Borba, C. E., Ribeiro, C., Espinoza, F. R. et al. (2016). Monolayer-multilayer adsorption phenomenological model: Kinetics, equilibrium and thermodynamics. *Chemical Engineering Journal, 284,* 1328–1341. DOI 10.1016/j.cej.2015.09.085.
38. Kang, F., Shi, C., Li, W., Eqi, M., Liu, Z. et al. (2022). Honeycomb like CdS/sulphur-modified biochar composites with enhanced adsorption-photocatalytic capacity for effective removal of rhodamine B. *Journal of Environmental Chemical Engineering, 10(1),* 106942. DOI 10.1016/j.jece.2021.106942.
39. Pietrzak, R., Nowicki, P., Kaźmierczak, J., Kuszyńska, I., Goscianska, J. et al. (2014). Comparison of the effects of different chemical activation methods on properties of carbonaceous adsorbents obtained from cherry stones. *Chemical Engineering Research and Design, 92(6),* 1187–1191. DOI 10.1016/j.cherd.2013.10.005.
40. Mahmoud, D. K., Salleh, M. A. M., Karim, W. A. W. A., Idris, A., Abidin, Z. Z. (2012). Batch adsorption of basic dye using acid treated kenaf fibre char: Equilibrium, kinetic and thermodynamic studies. *Chemical Engineering Journal, 181,* 449–457. DOI 10.1016/j.cej.2011.11.116.
41. Yang, G., Song, S., Li, J., Tang, Z., Ye, J. et al. (2019b). Preparation and $CO_2$ adsorption properties of porous carbon by hydrothermal carbonization of tree leaves. *Journal of Materials Science & Technology, 35(5),* 875–884. DOI 10.1016/j.jmst.2018.11.019.
42. Wang, Y., Liu, R. (2017). Comparison of characteristics of twenty-one types of biochar and their ability to remove multi-heavy metals and methylene blue in solution. *Fuel Processing Technology, 160,* 55–63. DOI 10.1016/j.fuproc.2017.02.019.
43. Lin, Y. C., Ho, S. H., Zhou, Y., Ren, N. Q. (2018). Highly efficient adsorption of dyes by biochar derived from pigments-extracted macroalgae pyrolyzed at different temperature. *Bioresource Technology, 259(3),* 104–110. DOI 10.1016/j.biortech.2018.02.094.
44. Fan, S., Wang, Y., Wang, Z., Tang, J., Tang, J. et al. (2017). Removal of methylene blue from aqueous solution by sewage sludge-derived biochar: Adsorption kinetics, equilibrium, thermodynamics and mechanism. *Journal of Environmental Chemical Engineering, 5(1),* 601–611. DOI 10.1016/j.jece.2016.12.019.
45. Cheng, J., Gu, J. J., Tao, W., Wang, P., Liu, L. et al. (2019). Edible fungus slag derived nitrogen-doped hierarchical porous carbon as a high-performance adsorbent for rapid removal of organic pollutants from water. *Bioresource Technology, 294,* 122149. DOI 10.1016/j.biortech.2019.122149.
46. Lee, D. S., Riedl, C., Krauss, B., Klitzing, K., Starke, U. et al. (2008). Raman spectra of epitaxial graphene on SiC and of epitaxial graphene transferred to $SiO_2$. *Nano Letters, 8(12),* 4320–4325. DOI 10.1021/nl802156w.
47. Huang, X., Cui, B., Ma, Y., Yan, X., Xia, L. et al. (2019). Three-dimensional nitrogen-doped mesoporous carbon nanomaterials derived from plant biomass: Cost-effective construction of label-free electrochemical aptasensor for sensitively detecting alpha-fetoprotein. *Analytica Chimica Acta, 1078,* 125–134. DOI 10.1016/j.aca.2019.06.009.

48. Ding, Z., Wan, Y., Hu, X., Wang, S., Zimmerman, A. R. et al. (2016). Sorption of lead and methylene blue onto hickory biochars from different pyrolysis temperatures: Importance of physicochemical properties. *Journal of Industrial and Engineering Chemistry, 37,* 261–267. DOI 10.1016/j.jiec.2016.03.035.
49. Li, J., Liang, N., Jin, X., Zhou, D., Li, H. et al. (2017). The role of ash content on bisphenol A sorption to biochars derived from different agricultural wastes. *Chemosphere, 171,* 66–73. DOI 10.1016/j.chemosphere.2016.12.041.
50. Güzel, F., Sayğılı, H., Sayğılı, G. A., Koyuncu, F., Yılmaz, C. (2017). Optimal oxidation with nitric acid of biochar derived from pyrolysis of weeds and its application in removal of hazardous dye methylene blue from aqueous solution. *Journal of Cleaner Production, 144(4),* 260–265. DOI 10.1016/j.jclepro.2017.01.029.
51. Gupta, V. K., Jain, R., Siddiqui, M. N., Saleh, T. A., Agarwal, S. et al. (2010). Equilibrium and thermodynamic studies on the adsorption of the dye rhodamine-B onto mustard cake and activated carbon. *Journal of Chemical & Engineering Data, 55(11),* 5225–5229. DOI 10.1021/je1007857.
52. Li, Z. T., Wu, H. T., Chen, W. Y., He, F. A., Li, D. H. (2019). Preparation of magnetic superhydrophobic melamine sponges for effective oil-water separation. *Separation and Purification Technology, 212(30),* 40–50. DOI 10.1016/j.seppur.2018.11.002.
53. Lee, K. T., Cheng, C. L., Lee, D. S., Chen, W. H., Vo, D. N. et al. (2022). Spent coffee grounds biochar from torrefaction as a potential adsorbent for spilled diesel oil recovery and as an alternative fuel. *Energy, 239(3),* 122467. DOI 10.1016/j.energy.2021.122467.
54. Liu, R. L., Liu, Y., Zhou, X. Y., Zhang, Z. Q., Zhang, J. et al. (2014). Biomass-derived highly porous functional carbon fabricated by using a free-standing template for efficient removal of methylene blue. *Bioresource Technology, 154(6),* 138–147. DOI 10.1016/j.biortech.2013.12.034.
55. Atun, G., Sismanoglu, T. (1996). Adsorption of 4, 4'-iso propylidene diphenol and diphenylolpropane 4, 4'dioxyaceticacid from aqueous solution on kaolinite. *Journal of Environmental Science & Health Part A, 31(8),* 2055–2069. DOI 10.1080/10934529609376474.